pubs.acs.org/Biomac

Article

Fabrication and Enhanced Flexibility of Starch-Based Cross-Linked Films

Ji-Hyun Cho, Kwang-Hyun Ryu, Hyun-Joong Kim,* and Jong-Ho Back*

Cite This: *Biomacromolecules* 2024, 25, 7894−7903

Read Online

ACCESS | Metrics & More | Article Recommendations

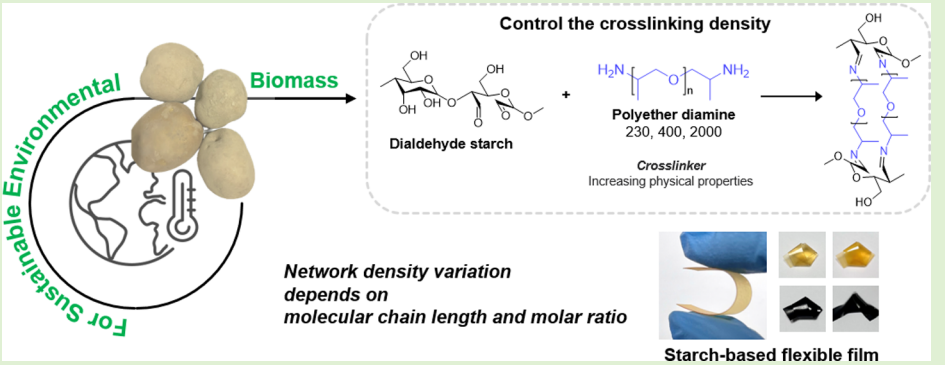

ABSTRACT: The development of sustainable materials has driven significant interest in starch as a renewable and biodegradable polymer. However, the inherent brittleness, hydrophilicity, and lack of thermoplasticity of native starch limit its application in material science. This study addresses the limitations of native starch by converting it to dialdehyde starch (DAS) and cross-linking with polyether diamines via imine bonds. The effects of Jeffamine molecular weights (D-2000, D-400, and D-230) and mole ratios on the mechanical, thermal, and structural properties of starch-based films were examined. The cross-linked DAS/Js films exhibited significant enhancements in flexibility and toughness. Specifically, DAS/J2000 at a 0.03 mol ratio achieved a tensile strength of 62.9 MPa. In comparison, DAS/J400 at a 0.5 mol ratio demonstrated 126.2% elongation at break, indicating the balance between cross-linking density and chain mobility. X-ray diffraction (XRD) analysis revealed reduced crystallinity and tighter molecular packing with increased cross-linking. Dynamic mechanical analysis (DMA) indicated a decrease in Tg with an increasing mole ratio, reflecting enhanced molecular mobility. The results underscore the potential of optimized cross-linking conditions to produce starch-based films with properties that contribute to developing sustainable biopolymer materials.

1. INTRODUCTION

Environmental concerns have significantly increased interest in starch as a promising natural polymer for sustainable material applications.[1,2] As a fully biodegradable polysaccharide derived from plants, starch offers several key advantages, including low cost, abundance, and wide availability from agricultural sources.[3−7] However, the application of native starch is limited by inherent drawbacks. The primary challenges include (a) its hydrophilicity (starch contains hydroxyl groups that make it water-sensitive, leading to the dissolution of amylopectin and the swelling of amylose, which degrade material properties upon moisture exposure) and (b) its lack of thermoplasticity (native starch undergoes thermal degradation at approximately 220 °C, before reaching its melting point of 240 °C, making it unstable under various humidity, temperature, and shear conditions).[8,9] As a result, native starch must be modified, particularly for applications beyond use as a filler in reinforcement plastics.[10−12]

Modification is required to develop starch as an alternative to petroleum-based plastics. This process alters the inherent properties of native starch, particularly its high water vapor permeability and poor mechanical properties. One effective approach is to plasticize starch, transforming it into thermoplastic starch (TPS) through physical and chemical processes. These modifications disrupt the intermolecular interactions within starch, weakening its structure and increasing the mobility of chains in the amorphous regions, thereby improving functionality and processability.[13−15] Physical modification is a simple and cost-effective method that

Received: August 27, 2024
Revised: October 22, 2024
Accepted: October 22, 2024
Published: November 6, 2024

involves the application of moisture, heat, and shear. Extrusion, a widely used plastic processing technique, combines thermal and mechanical force to modify starch efficiently, significantly influencing the microstructure and mechanical properties of starch-based materials.[16−19] Additionally, chemical modification, including cross-linking and derivatization, introduces functional groups into the starch polymer, overcoming the inherent drawbacks of native starch and leading to significant changes in its physicochemical properties.[20−25] Despite ongoing advancements in starch modification, starch-based materials still face challenges in mechanical performance, moisture resistance, and scalability due to their intrinsic brittleness, moisture sensitivity, and incompatibility with hydrophobic polymers. Continued research is necessary to address these challenges and expand the commercial applicability of starch-based materials.

To address these limitations, various approaches have been studied to improve the mechanical strength of starch-based films. Dialdehyde starch (DAS), derived from sodium periodate oxidation, is a versatile material that can react with diamines through a Schiff-base reaction, offering a promising strategy for developing starch-based bioplastics. Through this reaction, DAS forms a cross-linking network with diamine, which improves the mechanical properties of the material.[26−30] Jeffamine, a flexible polyether diamine, is particularly well-suited for enhancing the mechanical properties of starch-based films due to its inherent structure. It consists of a poly(propylene glycol) (PPG) backbone, which provides inherent flexibility through the rotational freedom of its polyether chains and is terminated by primary amine groups on both ends.[31−34] This dual-function structure allows Jeffamine to significantly improve the toughness and flexibility of starch-based films, addressing the brittleness commonly associated with starch-based materials. The presence of flexible polyether segments reduces rigidity, while the primary amine groups enable effective cross-linking with DAS. While previous studies have focused on increasing tensile strength, brittleness remains a challenge.

This study aims to determine the influence of molecular weight and the mole ratio of Jeffamine on the mechanical properties of DAS-based cross-linked films. This research provides insights into achieving a more balanced mechanical performance in starch-based bioplastics by analyzing how Jeffamine chain length and DAS/Jeffamine molar ratios affect these properties, thereby enhancing the potential applications of starch films, such as in biodegradable packaging, agricultural films, and biomedical materials, by addressing their inherent limitations.

2. EXPERIMENTAL SECTION

2.1. Materials. Native potato starch (NPS) was supplied by Daesang Co., Ltd. (Seoul, Korea). The starch was dried at 60 °C for 12 h and stored in a dry environment. Sodium periodate (99.8%), ethanol (95.0%), sulfuric acid (95.0%), sodium hydroxide (98.0%), and 1% phenolphthalein solution were purchased from Samchun Chemical Co., Ltd. (Seoul, Korea). Poly(propylene glycol) bis(2-aminopropyl ether), which were Jeffamine D-series amines, D-2000 (2000 g/mol), D-400 (430 g/mol), and D-230 (230 g/mol) were obtained from Huntsman Corporation (Texas) and used as received.

2.2. Synthesis of Dialdehyde Starch. Sodium periodate was dissolved in distilled water to achieve a concentration of 0.3 mol/L. Native potato starch (NPS) was then dispersed in this solution at a concentration of 5% (dry weight), with a mole ratio of sodium periodate to starch set at 1.1. The reaction was maintained at 40 °C for 24 h. After the reaction, the starch slurry was filtered, and the product was washed with distilled water five times to remove the iodate. The resulting product was then cross-washed with ethanol to remove remaining water and dried at 60 °C for 12 h. This process yielded dialdehyde starch (DAS) with over 90% content.

2.3. Determination of Aldehyde Contents. The degree of substitution (DS) of hydroxyl groups by aldehyde groups in starch was determined using the method described by Hofreiter, Alexander, and Wolff (1955). In this procedure, 0.2 g of starch or dialdehyde starch (DAS) was dissolved in 10 mL of 0.25 mol/L NaOH at 70 °C for 2 min. The solution was rapidly cooled with cold water, and 15 mL of 0.125 mol/L sulfuric acid was added. A small amount of phenolphthalein indicator was then introduced, and the mixture was titrated with 0.1 mol/L NaOH until the end point at pH 7 was reached, confirmed by both color change and pH meter readings. The DS was calculated using eq 1. v_1 and v_2 represent the total volumes of NaOH and H2SO4 (L), respectively. w is the dry weight of the DAS (g). c_1 and c_2 indicate the concentrations of NaOH and H_2SO_4 (mol/L), respectively. The value of 161 is the average molecular weight of the repeat unit in DAS.

$$\text{DA}\,\% = \frac{v_1c_1 - 2v_2c_2}{w/161} \times 100 \tag{1}$$

2.4. Fabrication of DAS/Js Cross-Linked Film. Dialdehyde starch-based Jeffamine (DAS/Js) cross-linked films were prepared via a Schiff-base reaction. The DAS/Js cross-linked films were produced using Jeffamine D-2000, D-400, and D-230, with the numbers indicating the molecular weight of the respective Jeffamine. The molar ratio of the aldehyde group to the amine group was varied, with ratios set at 1:0.1, 0.3, 0.5, 0.7, and 1.0 for DAS/J230 and DAS/J400 cross-linked films, and at 1:0.01, 0.03, 0.05, 0.1, 0.3, 0.5, 0.7, and 1.0 for DAS/J2000 cross-linked films. The films were named according to their respective Jeffamine type and molar ratio, for example, DAS/J230 0.01 and DAS/J2000 0.03. As an example, the detailed preparation process for the DAS/J2000 0.03 film is as follows: first, Jeffamine D-2000 (0.03 molar ratio relative to that of DAS) was dissolved in a 50% ethanol solution. Separately, DAS was completely and homogeneously dissolved in distilled water at a concentration of 0.5 wt % using pulsed tip sonication (output power: 15%; frequency: 1 s on and 2 s off) until 100,000 Joules of energy was applied. After the DAS solution was cooled to room temperature, it was added to the Jeffamine solution and mixed under magnetic stirring. The resulting mixture was then poured into a poly(tetrafluoroethylene) (PTFE) dish and dried at room temperature to form the cross-linked film.

2.5. Characterization Methods. *2.5.1. Morphology and Chemical Structure Characterization. 2.5.1.1. Field-Emission Scanning Electron Microscopy (FE-SEM).* The structure of the starch granules and the surface morphology of the DAS/Js cross-linked films were observed using FE-SEM (SIGMA, Carl Zeiss). Prior to imaging, the samples were dried in a vacuum oven at 60 °C for 12 h to remove any residual moisture. Each sample was then precoated with a uniform layer of 99.99% pure platinum via ion sputtering to prevent electron charging during the FE-SEM measurement.

2.5.1.2. Nuclear Magnetic Resonance (^{1}H NMR). The molecular structure was determined by using ^{1}H NMR spectroscopy. A 600 MHz high-resolution NMR spectrometer (AVANCE III HD, Bruker) was used for the analysis. All ^{1}H NMR samples were measured at 25 °C in DMSO-d_6.

2.5.1.3. Fourier Transform Infrared Spectroscopy (FT-IR). The Fourier transform infrared (FT-IR) spectra of the blends were recorded by using a Nicolet iS20 FT-IR spectrometer (Thermo Fisher Scientific). All samples were measured in the range of 4000−500 cm^{-1} with a resolution of 2 cm^{-1} and 16 scans.

2.5.2. Mechanical Properties Analysis. 2.5.2.1. Texture Analyzer. Tensile tests of DAS/J400 (0.3−1.0) and DAS/J2000 (0.03−1.0) were conducted using a texture analyzer (TA-XT plus, Stable Micro Systems) with a crosshead rate of 5 mm/s at 25 °C. The DAS/Js films were cut into 5 mm × 50 mm strips (ASTM D882) for testing at 5 repetitions.

https://doi.org/10.1021/acs.biomac.4c01172
Biomacromolecules 2024, 25, 7894−7903

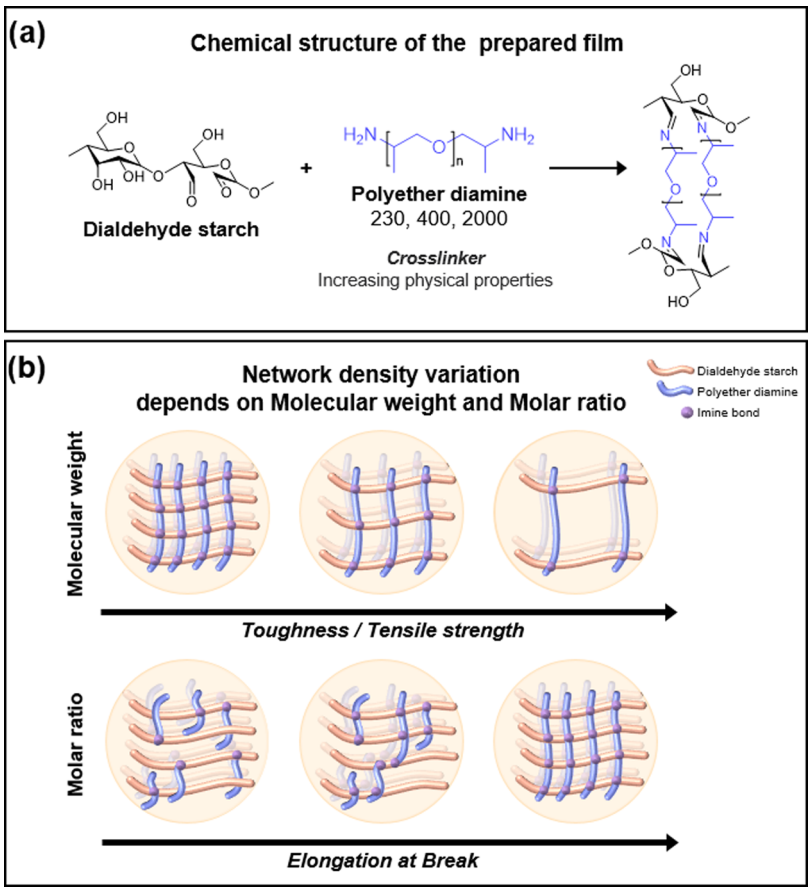

Figure 1. (a) Chemical structure of the starch materials and prepared film. (b) Schematic illustration for network density of prepared cross-linked film.

2.5.2.2. Dynamic Mechanical Analysis (DMA). DMA (Q800, TA Instruments) was used to assess the tan delta behavior in relation to the cross-link density of DAS/Js films. Film specimens of DAS/J400 (0.3−1.0) and DAS/J2000 (0.03−1.0) were prepared in dimensions of 6 × 30 mm. The measurements were conducted in film tension mode at 1% strain under a 1 Hz frequency, within a temperature range from −15 to 200 °C for DAS/J400 and from −60 to 220 °C for DAS/J2000, at a constant heating rate of 10 °C/min.

2.5.3. Cross-Linking Density Analysis. 2.5.3.1. X-Ray Diffraction (XRD). X-ray diffraction patterns were obtained using a micro X-ray scattering system (D8 Discover, Bruker) equipped with a Cu Kα radiation source (50 kV, 1000 μA) and a VANTEC500 detector. The XRD patterns were acquired over a 2θ angular range of 4−40°, with a step size of 0.02° and a step time of 600 s.

2.5.3.2. Gel Fraction. The gel content, which depends on the solvent solubility, was determined by using ethanol as the solvent. The gel fractions of the DAS/Js cross-linked films were measured by shaking the samples (15 mm × 15 mm) at 5 repetitions in ethanol for 3 days at room temperature. Afterward, the soluble fraction was removed by filtration, and the remaining gel was dried at 60 °C to a constant weight. The gel fraction was calculated using the following eq 2, where W_0 and W_1 represent the weights before and after filtration, respectively.

$$\text{gel fraction } (\%) = \frac{W_1}{W_0} \times 100 \tag{2}$$

2.5.4. Thermal Stability, Water Contact Angle, and Water Stability Test. 2.5.4.1. Thermogravimetric Analysis. Thermogravimetric analysis was performed using a TGA4000 analyzer (PerkinElmer). Approximately 10 mg of each specimen was heated from 30 to 600 °C at a rate of 10 °C/min.

2.5.4.2. Water Contact Angle. Analyzer (DAS 100, KRUSS) was used to determine surface wettability. Deionized water was used as the test liquid, and approximately 5 μm droplets were carefully placed on the dried film surface at 5 repetitions. Images were captured immediately after each droplet was applied to each sample.

2.5.4.3. Water Resistance. To evaluate the water resistance of the DAS/Js cross-linked films, a piece of film (5 mm × 5 mm) was soaked in 15 mL of water at room temperature for 7 days.

2.5.5. Statistical Analysis. All tests were conducted in 5 repetitions, and the resulting data were statistically analyzed using IBM SPSS Statistics 29 (SPSS Inc., Chicago, IL). A one-way analysis of variance (ANOVA) was performed, followed by Duncan's multiple range test ($p < 0.05$).

3. RESULTS AND DISCUSSION

3.1. Design Strategy. This study focuses on the development of biodegradable starch-based films by using starch as a renewable and sustainable resource. As illustrated in Figure 1a, starch was chemically modified into dialdehyde starch with a high degree of substitution (over 90%) to enable effective cross-linking with diamine of varying molecular weights (230, 400, 2000) at different mole ratios. The primary aim of this research is to refine the formation of starch-based films and adjust their mechanical properties for enhanced performance. By investigating the effect of cross-linking density as illustrated in Figure 1b, this study demonstrates how varying cross-linking density can affect the physical properties of films and tailor properties such as flexibility, toughness, and durability. This approach not only enables the development of starch-based materials suitable for diverse applications—

https://doi.org/10.1021/acs.biomac.4c01172
Biomacromolecules 2024, 25, 7894−7903

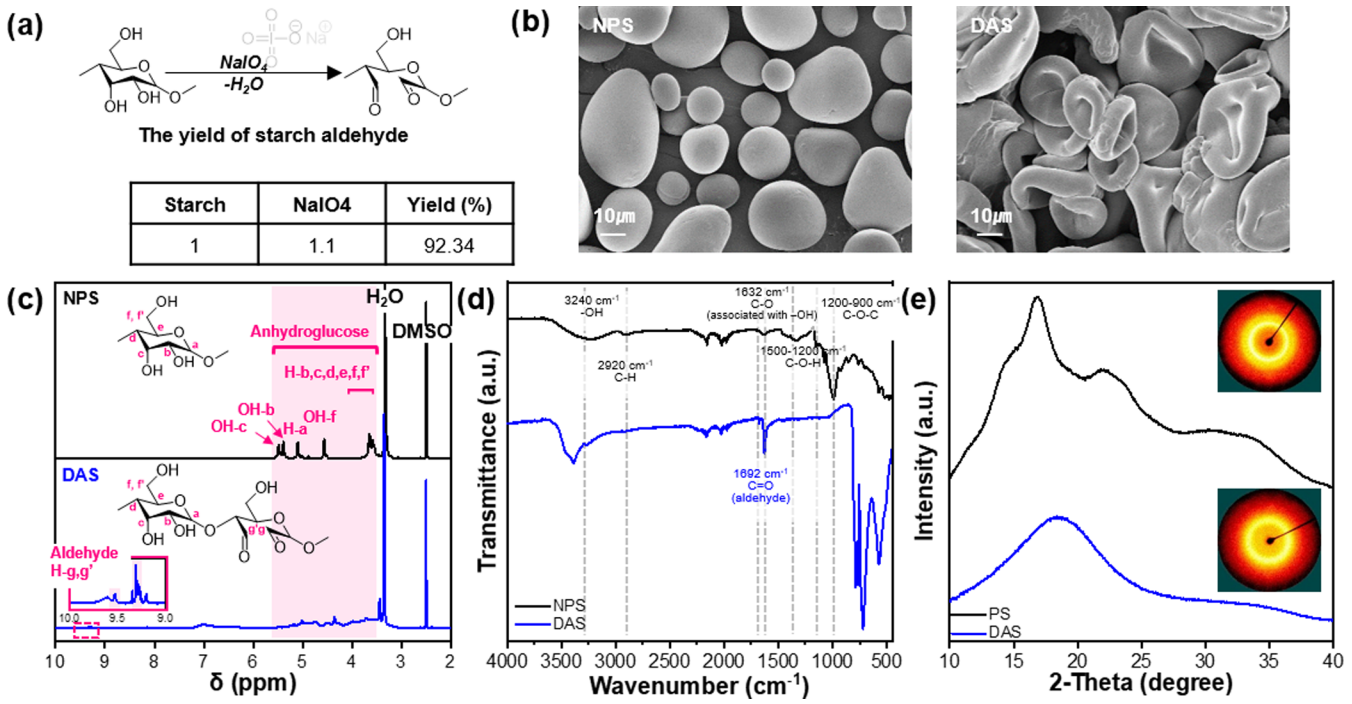

Figure 2. (a) Chemical structure of NPS and DAS and calculated degree of substitution, (b) SEM image, (c) ^{1}H NMR spectra, (d) FT-IR spectra, and (e) XRD spectra of NPS and modified DAS.

including biodegradable packaging and environmentally friendly coatings, but also aligns with broader sustainability.

3.2. Physical State Transformation of Starch. Native potato starch (NPS) was chemically modified to produce dialdehyde starch (DAS) with a high degree of substitution (over 90%) to enable efficient cross-linking. This modification, achieved through sodium periodate oxidation, ensures a sufficient concentration of reactive aldehyde groups necessary for cross-linking with diamines of varying molecular weights. The high aldehyde content of DAS is crucial for forming a stable and robust cross-linked network within the film matrix, thereby significantly enhancing the mechanical integrity and overall performance of the starch-based films. The degree of substitution (DS) of the aldehyde groups was determined using the rapid quantitative alkali consumption technique described by Hofreiter, Alexander, and Wolff,[35] confirming a DS of 92.34% (Figure 2a). To further understand the structural transformation resulting from the high aldehyde content, the physical changes in the DAS were analyzed using ^{1}H NMR, FT-IR, XRD, and SEM, providing comprehensive insights into the microstructure and cross-linking efficiency of the films.

Figure 2b presents SEM micrographs that illustrate the distinct granular morphology of NPS and DAS with a degree of substitution (DS) of 92.34%. The NPS granules display smooth rounded surfaces. This characteristic can be attributed to the compact and organized arrangement of amylopectin and amylose within the granules, which maintains their structural integrity. In contrast, the oxidative cleavage process used to produce DAS results in substantial morphological changes. The modified starch particles exhibit surface distortions and circular depressions, which can be attributed to the disruption of the granular structure due to the selective oxidation of amorphous regions.[36,37] Figure 2c exhibits the ^{1}H NMR spectra of NPS and DAS. The NPS spectrum shows characteristic signals corresponding to the anhydroglucose unit, with peaks observed at 5.49 ppm (OH-c), 5.38 ppm (OH-b), 5.09 ppm (H-a), 4.56 ppm (OH-f), and 3.63 to 3.57 ppm (H-b, c, d, e, f, f'). These signals are indicative of the hydroxyl groups and protons present in the native starch structure. After the modification to DAS, two new signals appear at 9.32 ppm (H-g) and 9.55 ppm (H-g'), corresponding to the aldehyde groups at positions C2 and C3 (HC2═O and HC3═O, respectively). The appearance of these new peaks confirms the successful conversion of NPS into DAS. In the FT-IR spectra (Figure 2d), the NPS exhibited characteristic peaks at O−H stretching (3346 cm^{-1}), C−H stretching (2920 cm^{-1}), C−O bending associated with the OH group (1632 cm^{-1}), C−O−C stretching (1146 cm^{-1}), C−O−H (1500−1200 cm^{-1}), and C−O−C bond (1200−900 cm^{-1}) attributed to the pyranose ring of glucose of stretching and vibration. The oxidation of starch by potassium periodate led to the linkage break at positions C2 and C3 of the anhydroglucose units. Therefore, a new absorption peak appeared at 1692 cm^{-1} related to the C═O stretching of the aldehyde functional group. The changes in crystallinity observed as NPS modified into DAS are presented in Figure 2e. The diffraction peaks of NPS appear at 2θ values of 14.5, 16.9, and 22.3°, corresponding to a typical B-type crystalline pattern, characteristic of potato starch.[38−40] In contrast, DAS shows no distinct peaks, indicating the absence of significant crystalline regions. This lack of clear diffraction peaks suggests that the long-range crystalline structure of the native starch has been effectively disrupted and destroyed during the modification process, resulting in an amorphous structure in the DAS.[41,42]

3.3. DAS/Js Cross-Linked Film Formation and Morphology Properties. The effects on the physical properties of the film and the cross-linking density were investigated by changing the molar ratio of polyether diamine (Jeffamine) with various molecular chain lengths (M_w 230,

https://doi.org/10.1021/acs.biomac.4c01172
Biomacromolecules 2024, 25, 7894−7903

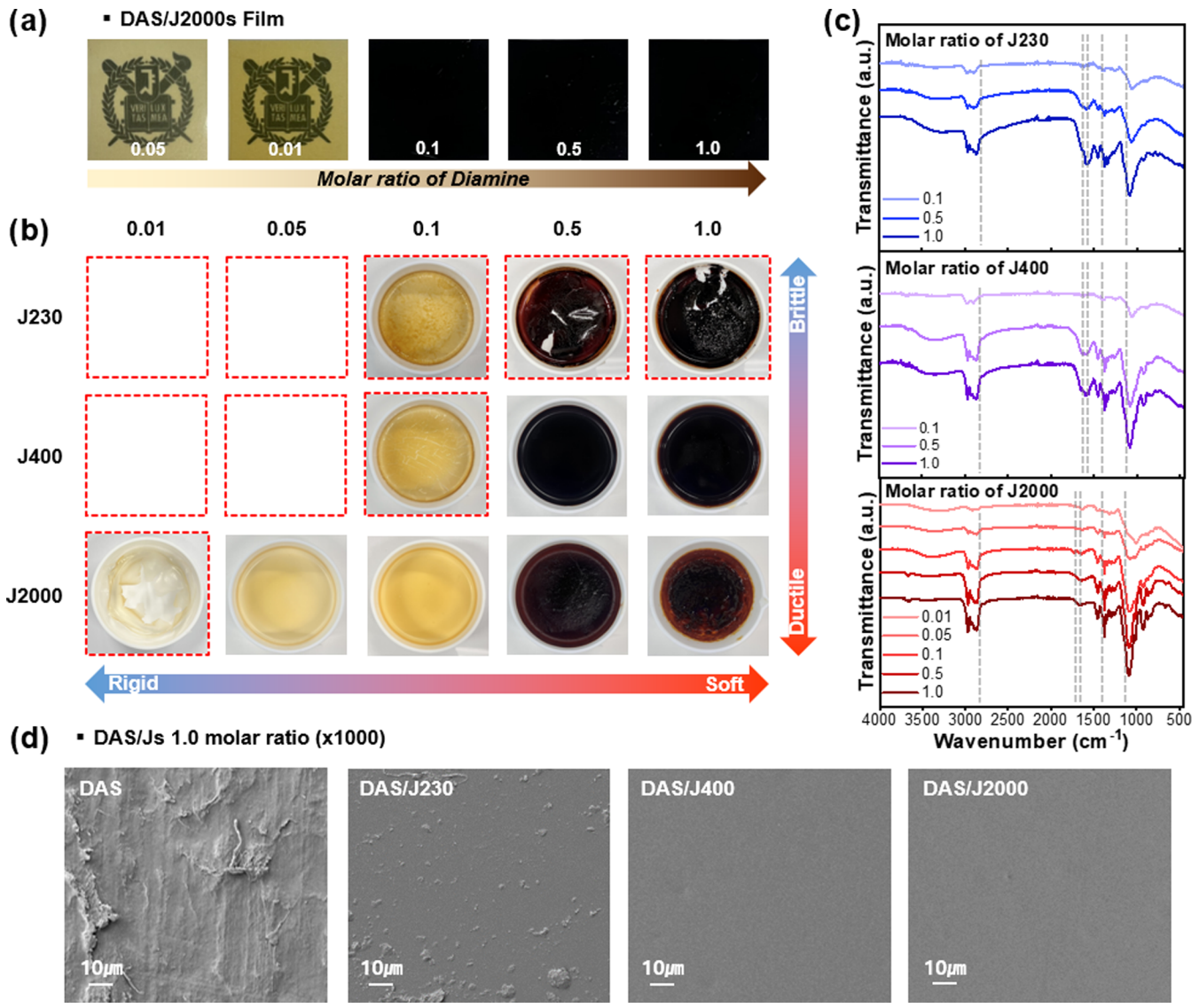

Figure 3. (a) Appearance of the prepared DAS/J2000s according to mole ratio, (b) photograph of film formation based on the mole ratio and molecular weight of Jeffamine, (c) FT-IR spectra of DAS/Js cross-linked films, and (d) SEM image of DAS/Js 1.0 mol ratio films.

400, 2000) as a cross-linker to form imine bonds in DAS. As shown in Figure 3a,b, the transparency of the films decreased and the color darkened as the molar ratio increased, regardless of the different molecular chain lengths of Jeffamine introduced into DAS. The higher cross-linking results in light scattering within the material, reducing clarity, and increased concentration of unreacted components, contributing to the darker appearance of the films.[43] The image in Figure 3b shows the variation in film formation behavior based on the molecular weight of the diamine and the molar ratio. Samples unable to form films are highlighted with red dotted box. When using the short molecular chain diamine J230, a low molar ratio of 0.1 resulted in brittle products due to insufficient network formation. Even at higher molar ratios (0.3−1.0), the short chain led to high cross-link density and excessive brittleness. For J400, film formation was only possible at higher molar ratios (0.3−1.0), where sufficient cross-linking occurred. In contrast, the longer and more flexible J2000 enabled film formation even at very low molar ratios (0.05) due to its ability to span greater distances and interact across multiple sites, maintaining network integrity with fewer cross-links. Consequently, shorter diamines such as J230 and J400 require higher molar ratios for film formation but result in relatively brittle products, while the longer J2000 forms flexible, cohesive films from lower molar ratios.

The FT-IR spectra presented in Figure 3c show that the stretching vibration peak of the aldehyde group at 1692 cm^{-1} decreases and eventually disappears in all DAS-Js cross-linked films, indicating the consumption of the aldehyde groups during the cross-linking reaction. Concurrently, new peaks emerge, including one at 1670 cm^{-1} corresponding to the imine bond (−C═N) and others at 2950 and 1260 cm^{-1}, which are attributed to the C−H stretching vibrations of the methylene group ($-CH_2-$) in Jeffamine. These spectral changes confirm the successful cross-linking between DAS and Jeffamine, evidenced by the formation of imine bonds and the incorporation of the diamine into the polymer network. The microstructure of the DAS/Js cross-linked film surfaces was examined using SEM (Figure 3d). The surface of the DAS film showed irregularities due to the destruction of starch granules, leaving loosely connected starch chains with weakened intermolecular interactions, resulting in an incom-

https://doi.org/10.1021/acs.biomac.4c01172
Biomacromolecules 2024, 25, 7894−7903

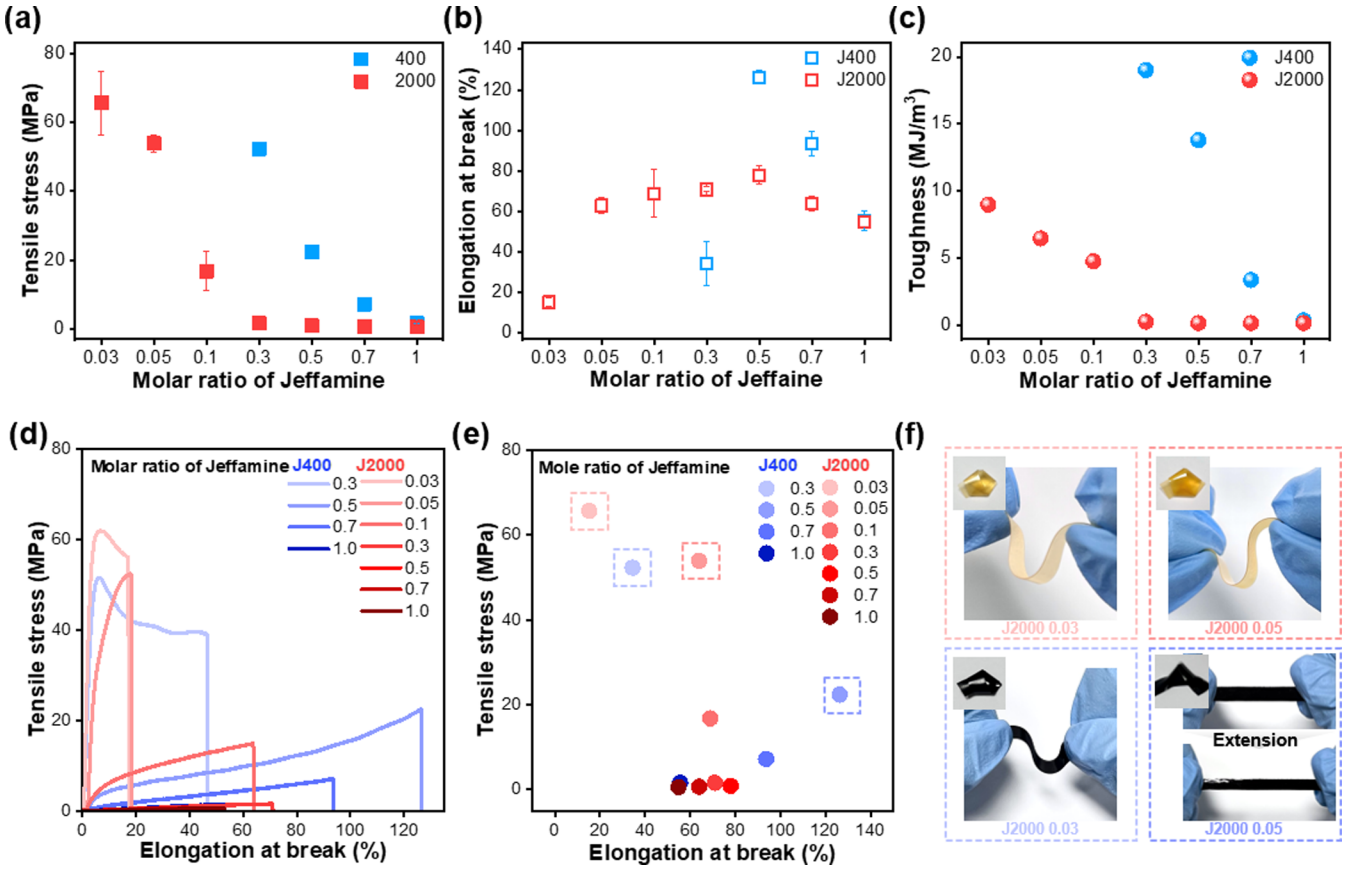

Figure 4. (a) Tensile strength, (b) elongation at break, (c) toughness, (d) strain curves, (e) range for the mechanical properties of DAS/J400 (0.3 to 1.0) and DAS/J2000 (0.03 to 1.0) films, and (f) photographs of the flexibility of the DAS/Js films.

Table 1. Mechanical Properties of DAS/J400 and DAS/J2000 Films Based on the Mole Ratio that Allows Film Formation

sample	molar ratio of Jeffamine	tensile stress (MPa)	Young's modulus (MPa)	elongation at break (%)	toughness (MJ/m^3)
DAS/J400	0.3	52.3 ± 1.3	1415.0 ± 36.5	34.4 ± 11.0	19.0
	0.5	22.4 ± 0.5	1006 ± 2.6	126.2 ± 3.3	16.8
	0.7	7.2 ± 0.4	15.7 ± 0.8	93.6 ± 5.9	3.4
	1.0	1.6 ± 0.1	3.8 ± 1.9	55.5 ± 4.8	0.4
	0.03	65.7 ± 9.3	1813.2 ± 171.4	15.2 ± 2.1	9.0
	0.05	53.9 ± 2.5	716.0 ± 82.9	62.9 ± 4.1	6.5
	0.1	16.8 ± 5.7	100.0 ± 5.0	68.9 ± 11.9	4.8
DAS/J2000	0.3	1.6 ± 0.1	2.3 ± 0.5	70.9 ± 1.2	0.3
	0.5	0.9 ± 0.1	2.3 ± 0.8	77.9 ± 4.5	0.2
	0.7	0.7 ± 0.1	2.1 ± 0.6	63.9 ± 3.8	0.2
	1.0	0.6 ± 0.1	1.2 ± 0.3	54.8 ± 2.6	0.2

plete network. In contrast, the DAS/Js 1.0 cross-linked films with a 1.0 molar ratio of Jeffamine displayed smoother surfaces. However, in the DAS/J230 1.0 film, the short Jeffamine chains failed to form a cohesive network, leading to surface roughness due to chain aggregation. On the other hand, the DAS/J400 1.0 and DAS/J2000 1.0 films, with longer molecular chains, effectively formed cross-linked networks with DAS, resulting in notably smooth surfaces.[44,45]

3.4. Physical Properties of DAS/Js Cross-Linked Film. Mechanical properties and film formation characteristics were evaluated using the samples that successfully formed films DAS/J400 (0.3−1.0) and DAS/J2000 (0.03−1.0). To assess the performance range of the DAS/Js cross-linked films, tensile property measurements were conducted, as shown in Figure 4. The DAS/J400 and DAS/J2000 samples, which formed films, exhibited similar mechanical behaviors across varying molar ratios.

As demonstrated in Figure 4a, the DAS/Js films with lower molar ratios demonstrated higher tensile strength, with DAS/J2000 at a 0.03 molar ratio achieving a tensile strength of 67.5 MPa, and DAS/J400 at a 0.3 molar ratio reaching 52.3 MPa. This trend could be attributed to the optimal balance between cross-linking density and molecular mobility, where the network is sufficiently rigid to resist deformation while retaining some flexibility. However, as the molar ratio of Jeffamine to DAS increases, a decrease in tensile strength is observed ($p < 0.05$). This reduction is due to the formation of a denser molecular network with higher cross-linking density, which restricts polymer chain mobility. The increased rigidity of the network results in a more brittle structure, making it

https://doi.org/10.1021/acs.biomac.4c01172
Biomacromolecules 2024, 25, 7894−7903

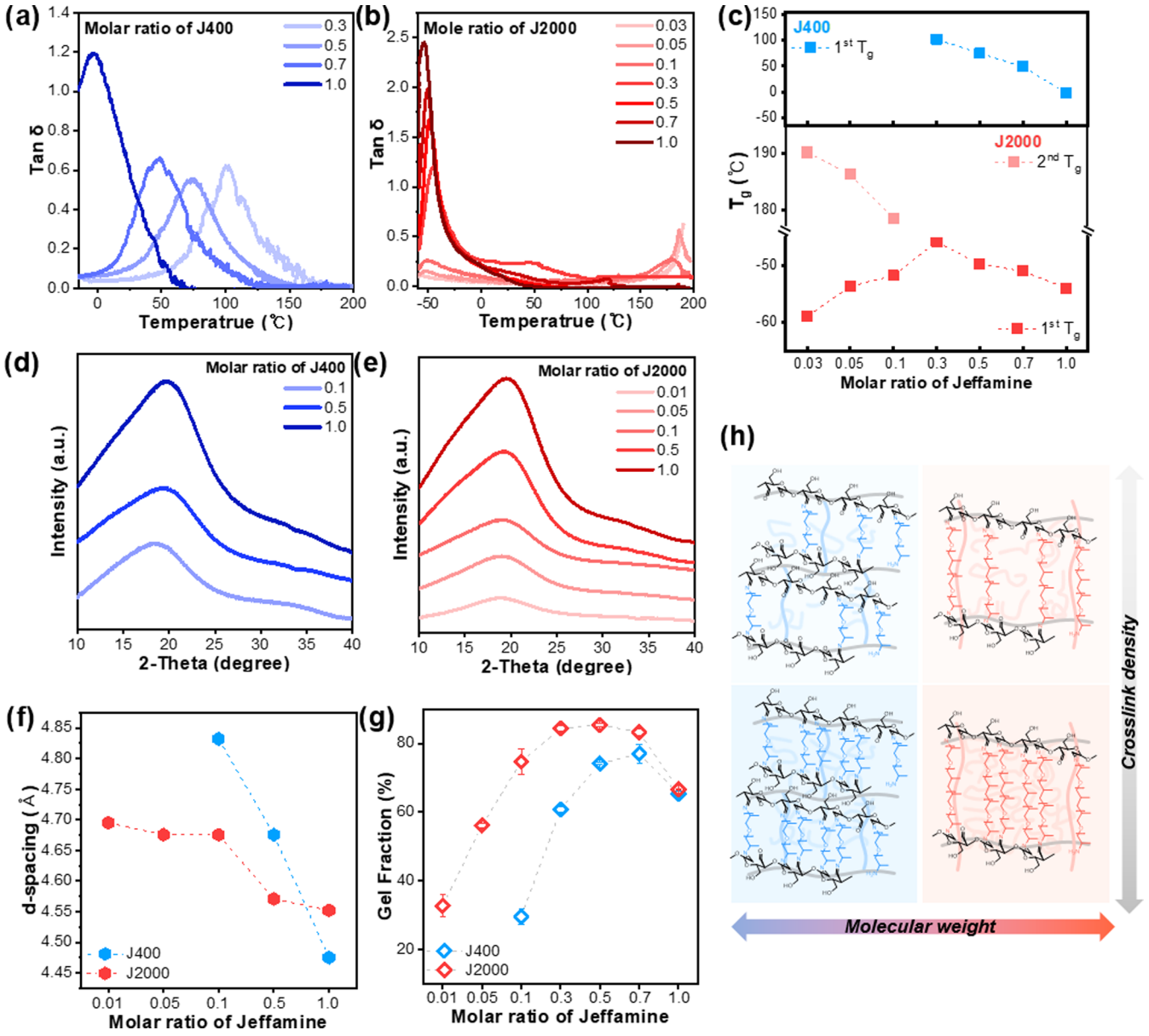

Figure 5. (a) Tan delta as a function of temperature of the DAS/J400s films. (b) Tan delta as a function of temperature of the DAS/J2000s films. (c) Glass transition temperature of the DAS/Js films measured by tan delta. (d) XRD spectra of DAS/J400s films. (e) XRD spectra of DAS/J2000s films. (f) Calculated *d*-spacing by 2θ, (g) gel fraction. (h) Schematic image of DAS/Js cross-linked films.

prone to fracture under tensile stress. As the cross-linked network becomes denser, the stress dissipation and absorption capacity of the material decreases, which lowers the overall tensile strength. The results for elongation at break, as shown in Figure 4b, indicate that elongation increases with the induced mole ratio of DAS to Jeffamine, reaching 126.2% for DAS/J400 at a 0.5 mol ratio and 77.9% for DAS/J2000 at a 0.5 mol ratio. However, beyond this point, elongation at break decreases in the DAS/Js cross-linked films, with DAS/J400 at a 1.0 mol ratio showing 55.5% and DAS/J2000 at a 1.0 mol ratio showing 54.8% elongation. The mole ratio of 0.7 appears to be the critical threshold for elongation at break. This phenomenon occurs because, as the cross-linking density increased, the flexibility and extendability of the molecular chains became increasingly constrained. Consequently, the network became more rigid, limiting the ability of the material to deform under stress without breaking. Toughness and Young's modulus both decreased with increasing mole ratio, a similar trend was observed in tensile strength (Figure 4c and Table 1). As the mole ratio increases, the dense cross-link network restricts chain mobility, reducing the ability of the material to absorb energy and deform plastically, leading to a significant decrease in toughness ($p < 0.05$). The increased cross-link density also introduces network heterogeneity, creating weak points that reduce stiffness and result in a lower Young's modulus. The stress−strain behavior of DAS/Js cross-linked films across different chain lengths and mole ratios is shown in Figure 4d,e. Lower mole ratios yield tougher films with higher tensile strength, while higher mole ratios result in softer films with reduced tensile strength due to overcross-linking. Films with longer Jeffamine chains exhibit higher tensile strength, whereas those with shorter chains represent greater elongation at break, attributed to increased chain flexibility. All DAS/Js cross-linked films maintained flexibility (Figure 4f), suggesting their

https://doi.org/10.1021/acs.biomac.4c01172
Biomacromolecules 2024, 25, 7894−7903

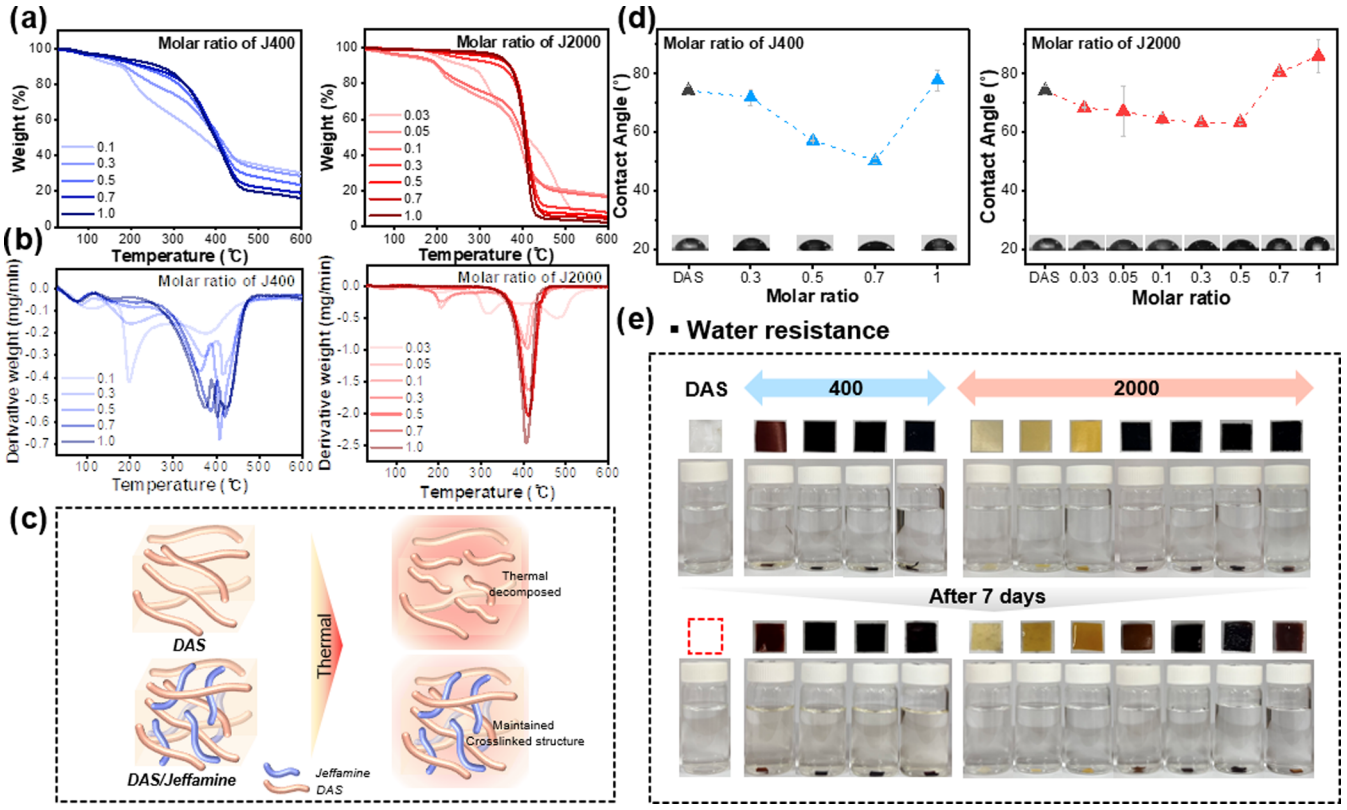

Figure 6. Thermal stability was measured by (a) TGA curves, (b) DTG curves, (c) schematic diagram of DAS and DAS/Js films, (d) water contact angle and droplet images, and (e) water resistance test of DAS/J400s and DAS/J2000s films.

potential to existing biobased and petroleum-based plastics, offering a range of applications.

3.5. Cross-Linked Network Properties of DAS/Js Film. Figure 5a–c presents T_g analysis via DMA, showing an overall decrease in T_g with increasing mole ratios of DAS/J400 and DAS/J2000 cross-linked films, indicative of enhanced molecular chain mobility. This trend suggests that the incorporation of Jeffamine into the relatively brittle DAS chains introduces greater flexibility into the network. However, in DAS/J2000 films with mole ratios between 0.03 and 0.1, two distinct T_g values (1st and second T_g) are observed at both low and high temperatures. This dual T_g behavior is likely due to phase separation or heterogeneous cross-linking at lower mole ratios, where the DAS and Jeffamine domains remain partially segregated. As the mole ratio increases beyond 0.3, T_g associated with the DAS domain decreases, indicating improved cross-linking efficiency. Ultimately, a single T_g was observed, suggesting that the DAS and Jeffamine components form a more homogeneous network. This transition to a single T_g signifies the effective integration of the two components, resulting in a more uniform cross-linked structure.

The XRD patterns and *d*-spacing analysis of DAS/Jeffamine cross-linked films, as shown in Figure 5d–f, demonstrate a clear trend where increasing the mole ratio reduces peak intensity, indicating a decrease in crystallinity. Both DAS/J400 and DAS/J2000 display an amorphous feature around the 20° peak, which becomes broader and less intense as cross-link density increases, reflecting the disruption of crystalline regions by the formation of a more amorphous network. Additionally, the *d*-spacing decreases with higher mole ratios, signifying tighter molecular packing within the matrix. This effect is more pronounced for the shorter J400 chains, which allow closer packing due to their smaller size, while the longer J2000 chains maintain greater flexibility, leading to a less pronounced reduction in *d*-spacing (Figure 5f). These structural changes, linked to the disruption of crystallinity and the formation of an amorphous network, correlate directly with the observed decrease in toughness, as the denser and less crystalline network restricts chain mobility, reducing the ability of the material to absorb energy and deform plastically. The gel fraction results presented in Figure 5g,h show that for DAS/J400 at a 0.7 mol ratio and DAS/J2000 at a 0.5 molar ratio, the increase in gel fraction corresponds to a rise in cross-link density, facilitating the formation of a stable network. This stability leads to a higher gel fraction and greater elongation at break, as the network remains strong, yet flexible enough to accommodate stretching. However, beyond a mole ratio of 0.5, the network becomes overcross-linked, resulting in rigidity that limits the ability of material to elongate, thereby reducing elongation at break. Additionally, excessive cross-linking introduces inhomogeneity, leading to incomplete network formation and a subsequent reduction in gel fraction. This behavior reflects the trend observed in the elongation at break, where both properties initially improve with increasing cross-linking, but then decrease with excessive cross-linking. The lower gel fraction of J400 compared to J2000 is due to the shorter molecular chains of J400, which create a less extensive and efficient cross-linked network, whereas the longer J2000 chains support more rigid network formation, resulting in a higher gel fraction at similar molar ratios.

3.6. Stability of DAS/Js Cross-Linked Films. Figure 6a,b illustrates the thermostability of DAS/Js cross-linked films as a function of varying mole ratios. As the mole ratio increases, the network becomes more densely and uniformly cross-linked,

https://doi.org/10.1021/acs.biomac.4c01172
Biomacromolecules 2024, 25, 7894–7903

leading to enhanced thermal stability. At lower mole ratios, the cross-link density is low, resulting in a heterogeneous network structure. This nonuniformity causes different regions of the material to decompose at varying temperatures, which is reflected in the presence of multiple DTG peaks corresponding to multiple stages of thermal decomposition. However, with increasing mole ratio, particularly in films cross-linked with higher molecular weight J2000 than J400, the cross-linked network becomes more uniform. This uniformity reduces the likelihood of early thermal degradation, leading to a single DTG peak indicative of a more cohesive decomposition process. The improved thermal stability, observed as the network becomes more homogeneous, is depicted schematically in Figure 6c. This enhanced stability underscores the critical role of cross-link density and uniformity in determining the thermal behavior of the cross-linked films.

The DAS film was compared with the fabricated DAS/Js cross-linked films to evaluate its water stability. The water contact angle as a function of the molar ratio for DAS/Js cross-linked films is shown in Figure 6d. For DAS/J400s, the water contact angle decreases to 50.3° at a 0.7 mol ratio and then rises to 77.7° at a 1.0 molar ratio. Similarly, for DAS/J2000s, the angle drops to 63.5° at a 0.5 molar ratio before increasing to 86.0° at a 1.0 molar ratio. This trend is attributed to the formation of a denser cross-linked network with an increasing molar ratio, which smooths the surface and reduces roughness, thereby lowering the water contact angle. However, at higher molar ratios, excessive cross-linking can lead to phase separation, resulting in hydrophobic Jeffamine segments that remain unbound to DAS and become exposed on the surface, which in turn raises the water contact angle due to increased surface hydrophobicity.[46,47] Meanwhile, water socked tests for 7 days (Figure 6e), although the DAS film degraded within hours, the DAS/Js cross-linked films exhibited strong water resistance despite their lower contact angles. This resistance is due to the dense cross-link network, which prevents water penetration and maintains the structural integrity of films even in a hydrophilic environment.

4. CONCLUSIONS

This study aimed to enhance film properties by cross-linking dialdehyde starch (DAS) with Jeffamine to expand the application of starch-based films. The starch was converted to DAS via sodium periodate oxidation to provide cross-linking. The effects of varying the Jeffamine molecular weight and molar ratio on the mechanical properties were examined. The results demonstrated distinct mechanical behaviors across the films, depending on molecular chain length and cross-linking density. Specifically, lower molar ratios yielded higher tensile strengths (DAS/J400 0.3 at 52.3 MPa, DAS/J2000 0.03 at 65.7 MPa) and optimal elongation at break (DAS/J400 0.5 at 126.2%, DAS/J2000 0.5 at 77.9%) due to a balanced cross-link density and chain mobility. However, increased molar ratios resulted in a more rigid network structure on films due to excessive cross-linking. XRD and *d*-spacing analyses confirmed reduced crystallinity and tighter molecular packing, particularly in films with shorter Jeffamine chains. The resulting DAS/Js cross-linked films exhibited enhanced thermal stability and water resistance, overcoming the limitations of traditional starch-based materials. Ultimately, this study underscores the potential of optimized cross-linking conditions to produce starch-based films with properties suitable for sustainable biopolymer applications.

AUTHOR INFORMATION

Corresponding Authors

Hyun-Joong Kim − *Laboratory of Adhesion & Bio-Composites, Department of Agriculture, Forestry and Bioresources, Seoul National University, Seoul 08826, Republic of Korea; Research Institute of Agriculture and Life Sciences, College of Agriculture and Life Sciences, Seoul National University, Seoul 08826, Republic of Korea;* orcid.org/0000-0002-3897-7939; Email: hjokim@snu.ac.kr

Jong-Ho Back − *Research Institute of Agriculture and Life Sciences, College of Agriculture and Life Sciences, Seoul National University, Seoul 08826, Republic of Korea;* orcid.org/0000-0003-4674-4710; Email: back1231@snu.ac.kr

Authors

Ji-Hyun Cho − *Laboratory of Adhesion & Bio-Composites, Department of Agriculture, Forestry and Bioresources, Seoul National University, Seoul 08826, Republic of Korea;* orcid.org/0009-0003-3371-3736

Kwang-Hyun Ryu − *Laboratory of Adhesion & Bio-Composites, Department of Agriculture, Forestry and Bioresources, Seoul National University, Seoul 08826, Republic of Korea*

Complete contact information is available at: https://pubs.acs.org/10.1021/acs.biomac.4c01172

Author Contributions

The manuscript was written through contributions of all authors. All authors have given approval to the final version of the manuscript.

Funding

This work was supported by the Technology Innovation Program (20017973, development of technology for commercialization of high starch content biodegradable composite material for flexible film) funded by the Ministry of Trade, Industry & Energy (MOTIE, Korea).

Notes

The authors declare no competing financial interest.

REFERENCES

(1) Surendren, A.; Mohanty, A. K.; Liu, Q.; Misra, M. A review of biodegradable thermoplastic starches, their blends and composites: Recent developments and opportunities for single-use plastic packaging alternatives. *Green Chem.* **2022**, *24* (22), 8606−8636.

(2) Jiang, T.; Duan, Q.; Zhu, J.; Liu, H.; Yu, L. Starch-based biodegradable materials: Challenges and opportunities. *Adv. Ind. Eng. Polym. Res.* **2020**, *3* (1), 8−18.

(3) Arvanitoyannis, I. S. Totally and partially biodegradable polymer blends based on natural and synthetic macromolecules: preparation, physical properties, and potential as food packaging materials. *J. Macromol. Sci., Part C: Polym. Rev.* **1999**, *39* (2), 205−271.

(4) Dupuis, J. H.; Liu, Q. Potato starch: a review of physicochemical, functional and nutritional properties. *Am. J. Potato Res.* **2019**, *96* (2), 127−138.

(5) Bardhan, S. K.; Gupta, S.; Gorman, M.; Haider, M. A. Biorenewable chemicals: Feedstocks, technologies and the conflict with food production. *Renewable Sustainable Energy Rev.* **2015**, *51*, 506−520.

(6) Ashogbon, A. O.; Akintayo, E. T. Recent trend in the physical and chemical modification of starches from different botanical sources: A review. *Starch* **2014**, *66* (1−2), 41−57.

(7) Pérez, S.; Bertoft, E. The molecular structures of starch components and their contribution to the architecture of starch granules: A comprehensive review. *Starch* **2010**, *62* (8), 389−420.
(8) Avérous, L. Biodegradable multiphase systems based on plasticized starch: a review. *J. Macromol. Sci., Part C: Polym. Rev.* **2004**, *44* (3), 231−274.
(9) Mary, S. K.; Koshy, R. R.; Arunima, R.; Thomas, S.; Pothen, L. A. A review of recent advances in starch-based materials: Bionanocomposites, pH sensitive films, aerogels and carbon dots. *Carbohydr. Polym. Technol. Appl.* **2022**, *3*, No. 100190.
(10) Bertoft, E. Understanding starch structure: Recent progress. *Agronomy* **2017**, *7* (3), 56.
(11) Tester, R. F.; Karkalas, J.; Qi, X. Starch-composition, fine structure and architecture. *J. Cereal Sci.* **2004**, *39* (2), 151−165.
(12) Kong, L.; Lee, C.; Kim, S. H.; Ziegler, G. R. Characterization of starch polymorphic structures using vibrational sum frequency generation spectroscopy. *J. Phys. Chem. B* **2014**, *118* (7), 1775−1783.
(13) Mohammadi Nafchi, A.; Moradpour, M.; Saeidi, M.; Alias, A. K. Thermoplastic starches: Properties, challenges, and prospects. *Starch* **2013**, *65* (1−2), 61−72.
(14) Wang, S.; Li, C.; Copeland, L.; Niu, Q.; Wang, S. Starch retrogradation: A comprehensive review. *Compr. Rev. Food Sci. Food Saf.* **2015**, *14* (5), 568−585.
(15) Montilla-Buitrago, C. E.; Gómez-López, R. A.; Solanilla-Duque, J. F.; Serna-Cock, L.; Villada-Castillo, H. S. Effect of plasticizers on properties, retrogradation, and processing of extrusion-obtained thermoplastic starch: A review. *Starch* **2021**, *73* (9−10), No. 2100060.
(16) Arvanitoyannis, I.; Nakayama, A.; Aiba, S.-i. Edible films made from hydroxypropyl starch and gelatin and plasticized by polyols and water. *Carbohydr. Polym.* **1998**, *36* (2−3), 105−119.
(17) Yu, L.; Christie, G. Microstructure and mechanical properties of orientated thermoplastic starches. *J. Mater. Sci.* **2005**, *40*, 111−116.
(18) Ojogbo, E.; Ogunsona, E. O.; Mekonnen, T. H. Chemical and physical modifications of starch for renewable polymeric materials. *Mater. Today Sustainability* **2020**, *7*−*8*, No. 100028.
(19) Fan, Y.; Picchioni, F. Modification of starch: A review on the application of "green" solvents and controlled functionalization. *Carbohydr. Polym.* **2020**, *241*, No. 116350.
(20) Wang, X.; Huang, L.; Zhang, C.; Deng, Y.; Xie, P.; Liu, L.; Cheng, J. Research advances in chemical modifications of starch for hydrophobicity and its applications: A review. *Carbohydr. Polym.* **2020**, *240*, No. 116292.
(21) Liu, H.; Sui, X.; Xu, H.; Zhang, L.; Zhong, Y.; Mao, Z. Self-healing polysaccharide hydrogel based on dynamic covalent enamine bonds. *Macromol. Mater. Eng.* **2016**, *301* (6), 725−732.
(22) Lewicka, K.; Siemion, P.; Kurcok, P. Chemical modifications of starch: microwave effect. *Int. J. Polym. Sci.* **2015**, *2015* (1), No. 867697.
(23) Imre, B.; Vilaplana, F. Organocatalytic esterification of corn starches towards enhanced thermal stability and moisture resistance. *Green Chem.* **2020**, *22* (15), 5017−5031.
(24) Nypelö, T.; Berke, B.; Spirk, S.; Sirviö, J. A. Periodate oxidation of wood polysaccharides—Modulation of hierarchies. *Carbohydr. Polym.* **2021**, *252*, No. 117105.
(25) Liu, H.; Guo, L.; Tao, S.; Huang, Z.; Qi, H. Freely moldable modified starch as a sustainable and recyclable plastic. *Biomacromolecules* **2021**, *22* (6), 2676−2683.
(26) Zhang, H.; Su, Z.; Wang, X. Starch-based rehealable and degradable Bioplastic enabled by dynamic imine chemistry. *ACS Sustainable Chem. Eng.* **2022**, *10* (26), 8650−8657.
(27) Taynton, P.; Yu, K.; Shoemaker, R. K.; Jin, Y.; Qi, H. J.; Zhang, W. Heat-or water-driven malleability in a highly recyclable covalent network polymer. *Adv. Mater.* **2014**, *26* (23), 3938−3942.
(28) Taynton, P.; Ni, H.; Zhu, C.; Yu, K.; Loob, S.; Jin, Y.; Qi, H. J.; Zhang, W. Repairable woven carbon fiber composites with full recyclability enabled by malleable polyimine networks. *Adv. Mater.* **2016**, *28* (15), 2904−2909.
(29) Zou, Z.; Zhu, C.; Li, Y.; Lei, X.; Zhang, W.; Xiao, J. Rehealable, fully recyclable, and malleable electronic skin enabled by dynamic covalent thermoset nanocomposite. *Sci. Adv.* **2018**, *4* (2), No. eaaq0508.
(30) Christensen, P. R.; Scheuermann, A. M.; Loeffler, K. E.; Helms, B. A. Closed-loop recycling of plastics enabled by dynamic covalent diketoenamine bonds. *Nat. Chem.* **2019**, *11* (5), 442−448.
(31) Gosnell, R. B.; Levine, H. H. Some effects of structure on a polymer's performance as a cryogenic adhesive. *J. Macromol. Sci., Chem.* **1969**, *3* (7), 1381−1393.
(32) Shan, L.; Verghese, K.; Robertson, C.; Reifsnider, K. Effect of network structure of epoxy DGEBA-poly (oxypropylene) diamines on tensile behavior. *J. Polym. Sci., Part B: Polym. Phys.* **1999**, *37* (19), 2815−2819.
(33) Yang, G.; Fu, S.-Y.; Yang, J.-P. Preparation and mechanical properties of modified epoxy resins with flexible diamines. *Polymer* **2007**, *48* (1), 302−310.
(34) Brancart, J.; Verhelle, R.; Mangialetto, J.; Van Assche, G. Coupling the microscopic healing behaviour of coatings to the thermoreversible Diels-Alder network formation. *Coatings* **2019**, *9* (1), 13.
(35) Hofreiter, B. T.; Alexander, B.; Wolff, I. Rapid estimation of dialdehyde content of periodate oxystarch through quantitative alkali consumption. *Anal. Chem.* **1955**, *27* (12), 1930−1931.
(36) Fiedorowicz, M.; Para, A. Structural and molecular properties of dialdehyde starch. *Carbohydr. Polym.* **2006**, *63* (3), 360−366.
(37) Yu, J.; Chang, P. R.; Ma, X. The preparation and properties of dialdehyde starch and thermoplastic dialdehyde starch. *Carbohydr. Polym.* **2010**, *79* (2), 296−300.
(38) Dankar, I.; Haddarah, A.; Omar, F. E.; Pujolà, M.; Sepulcre, F. Characterization of food additive-potato starch complexes by FTIR and X-ray diffraction. *Food Chem.* **2018**, *260*, 7−12.
(39) Ribotta, P. D.; Cuffini, S.; León, A. E.; Añón, M. C. The staling of bread: an X-ray diffraction study. *Eur. Food Res. Technol.* **2004**, *218*, 219−223.
(40) Ispas-Szabo, P.; Ravenelle, F.; Hassan, I.; Preda, M.; Mateescu, M. A. Structure−properties relationship in cross-linked high-amylose starch for use in controlled drug release. *Carbohydr. Res.* **1999**, *323* (1−4), 163−175.
(41) Li, Y.; Wang, J.-H.; Han, Y.; Yue, F.-H.; Zeng, X.-A.; Chen, B.-R.; Zeng, M.-Q.; Woo, M.-W.; Han, Z. The effects of pulsed electric fields treatment on the structure and physicochemical properties of dialdehyde starch. *Food Chem.* **2023**, *408*, No. 135231.
(42) Wang, P.; Wang, Y.; Hong, P.; Zhou, C. Di-aldehyde starch crystal: A novel bio-crosslinker for strengthening the structure and physio-chemical properties of gelatin-based films. *Food Biosci.* **2021**, *43*, No. 101308.
(43) Liu, Y.; Xing, Y.; Zhang, Y.; Guan, S.; Zhang, H.; Wang, Y.; Wang, Y.; Jiang, Z. Novel soluble fluorinated poly (ether imide) s with different pendant groups: synthesis, thermal, dielectric, and optical properties. *J. Polym. Sci., Part A: Polym. Chem.* **2010**, *48* (15), 3281−3289.
(44) Wang, Y.; Ma, H.; Ying, S.; Gao, J.; Zhou, X. Effect of dialdehyde starch on cassava starch/poly (vinyl alcohol) blends fabricated by melt mixing method with glycerol plasticized. *J. Appl. Polym. Sci.* **2024**, *141* (37), No. e55932.
(45) Ciaccia, M.; Di Stefano, S. Mechanisms of imine exchange reactions in organic solvents. *Org. Biomol. Chem.* **2015**, *13* (3), 646−654.
(46) Shao, H.; Sun, H.; Yang, B.; Zhang, H.; Hu, Y. Facile and green preparation of hemicellulose-based film with elevated hydrophobicity via cross-linking with citric acid. *RSC Adv.* **2019**, *9* (5), 2395−2401.
(47) Liu, X.; Chen, W.; Gustafson, C. T.; Miller II, A. L.; Waletzki, B. E.; Yaszemski, M. J.; Lu, L. Tunable tissue scaffolds fabricated by in situ crosslink in phase separation system. *RSC Adv.* **2015**, *5* (122), 100824−100833.

https://doi.org/10.1021/acs.biomac.4c01172
Biomacromolecules 2024, 25, 7894−7903